Spectroscopic Investigation and Theoretical Modeling of Benzothiadiazole-Based Charge-Transfer Chromophores: from Solution to Nanoaggregates

Spectroscopic Investigation and Theoretical Modeling of Benzothiadiazole-Based Charge-Transfer Chromophores: from Solution to Nanoaggregates

Brunella Bardi,[1] *Chunxiang Dall'Agnese,*[2,3] *Kathleen I. Moineau-Chane Ching,*[2,3,*] *Anna Painelli,*[1] *Francesca Terenziani*[1,*]

[1] Dipartimento di Scienze Chimiche, della Vita e della Sostenibilità Ambientale, Università di Parma, Parco Area delle Scienze 17/a, I-43124 Parma, Italy

[2] CNRS; LCC (Laboratoire de Chimie de Coordination); 205 route de Narbonne, F-31077 Toulouse, France

[3] Université de Toulouse; UPS, INP; LCC; F-31077 Toulouse, France

AUTHOR INFORMATION

Corresponding Author

*E-mail: kathleen.chane@lcc-toulouse.fr; Tel: +33 (0)5 61333133.

*E-mail: francesca.terenziani@unipr.it; Tel: +39 0521 905453.

ABSTRACT

Experimental and theoretical investigations are presented on four quadrupolar molecules constituted of a central electron-acceptor 2,1,3-benzothiadiazole conjugated at both sides with electron-donating thiophene (or 2,2'-bithiophene) substituted groups. Former investigation of their physico-chemical properties demonstrated that thermally induced self-organization might be achieved for one of them. In this study, we further explore the structure-properties relationships for these quadrupolar chromophores also examining their aggregation behavior in organic nanoparticles. Strong spectroscopic evidence of J-aggregates formation is obtained, favored by the presence of branched terminal alkyl chains. The surprisingly low fluorescence quantum yield of these J-aggregates is rationalized within the essential-state model approach.

INTRODUCTION

Charge-transfer (CT) dyes are a large family of molecular systems containing electron donor (D) and acceptor (A) groups linked via π-conjugated bridges, coming in a wide variety of structures, for example dipolar (DA), quadrupolar (DAD or ADA) and octupolar (AD_3 or DA_3). CT dyes have been extensively studied for functional applications.[1,2] The low-energy photophysics of π-conjugated dyes with donor/acceptor groups is dominated by intramolecular charge transfer, resulting in low-frequency transitions, usually in the visible range, with large transition dipole moments.[3–5] These systems are of interest for organic light emitting diodes,[6–8] photovoltaic cells,[9–12] liquid crystals and more,[13,14] and also in electronics, for example in thin film transistors.[15,16] Multipolar chromophores are known for their interesting nonlinear optical properties, such as two-

photon absorption (2PA),[17–20] making them promising for biomedical applications, including microscopy and photodynamic therapy.[21,22] Most CT dyes, however, are poorly soluble in water, thus limiting their potential exploitation in the biological applications. Strategies to achieve good biocompatibility of these dyes include the preparation of stable Organic Nanoparticle (ONPs) suspensions in aqueous media,[23–25] provided they retain the properties of interest.

Aggregation strongly affects the optical properties of dyes, sometimes enhancing the fluorescence,[26–29] and/or the 2PA cross-section,[30–32] making the nanoaggregates good probes for multiphoton fluorescence microscopy and in-vivo imaging.[33–38] Adverse aggregation effects on optical properties are also possible, however, and are fairly common, indeed, making the design of functional molecular materials a challenging task.[39–43] It is therefore important to obtain a sound understanding of aggregation effects as to be able to exploit the opportunity offered by the supramolecular organization of dyes towards optimized optical properties for the sought applications.

Theoretical models represent a valuable tool for gaining insight into the spectroscopic behavior of CT systems, offering guidelines to the engineering of new molecules with improved optical linear and nonlinear responses.[44–47] In this framework, essential-state models (ESMs) represent an alternative and reliable approach to traditional first-principle calculations for drawing structure-properties relationships.[48,49] ESMs are semi-empirical in nature and describe the low-energy spectroscopy of a chromophore by means of a limited number of states, corresponding to its main resonating structures. The few parameters entering the model are extracted from experimental data and, once defined, can be used to reliably predict other properties. ESMs have been developed for dipolar,[50] quadrupolar[51] and octupolar[52] chromophores, and have been extended in order to account for electron-vibration coupling as well as for polar solvation.[53] These models have been

extensively validated against experiment, and have shown a predictive accuracy, concerning complex phenomena such as symmetry breaking.[51,54,55] ESMs proved also effective in the description of linear and nonlinear properties of multichromophores,[56–58] as well as molecular assemblies of dipolar[59–62] and quadrupolar[63,64] dyes, where intermolecular interactions give rise to collective and cooperative effects that, in highly polarizable dyes, lead to the failure of the classical exciton theory.[59,62,64]

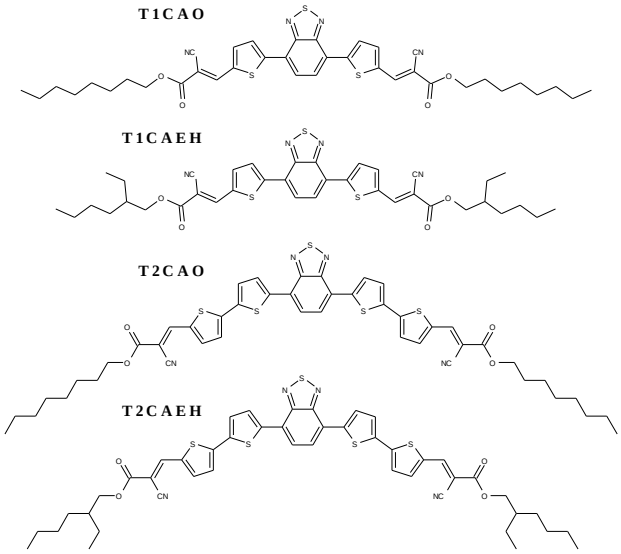

Figure 1. Molecular structures of the investigated compounds.

In this work, we will focus on the four chromophores presented in Figure 1. The central electron-acceptor 2,1,3-benzothiadiazole is conjugated at both sides with two electron-donating thiophene (or 2,2'-bithiophene) substituted moieties, in a D-A-D motif. End-capping with alkyl-cyanoacetate groups improves the solubility and optoelectronic properties of the compounds (e.g. a fine tuning of the optical spectral window and frontier molecular orbitals), making them promising semiconducting materials for organic photovoltaics.[65,66] The alkyl-cyanoacetate groups can be considered by themselves as electron withdrawing groups, but we will satisfactorily reproduce the

properties of the molecules at hand describing them in terms of a simple D-A-D motif (the donors being constituted by the end-capped thiophene or bithiophene moieties). The nature of the alkyl chains (linear – octyl – or branched – ethylhexyl) governs self-organization of the chromophores in the solid state, but marginally affects the optical properties of the solvated dyes.[66]

In the first part of this paper, we will present a detailed spectroscopic characterization of the dyes in solution, where intermolecular interactions are negligible. Then we will address their aggregation, reporting the preparation and characterization of ONP suspensions in water. Experimental data suggest the ability of the chromophores to arrange in partially ordered J-aggregates, whose fluorescence is however surprisingly low. The formation of such "non-fluorescent J-aggregates" is a phenomenon already observed for other systems, for example squaraine dyes[67] and porphyrin derivatives.[68] The second part of this work is devoted to the definition of ESMs for the target compounds in solution, based on the three-state model developed for quadrupolar chromophores.[51] Model parameters are extracted from experimental room-temperature spectra and are further validated against low-temperature data. In a bottom-up modeling approach, we then extend the ESMs to aggregates, and use them to successfully rationalize the spectral properties of ONPs.

EXPERIMENTAL SECTION

Synthesis. The synthesis of the four investigated compounds was achieved through a ligand-less direct arylation step followed by a double Knoevenagel condensation, as reported elsewhere.[66] The synthesis of **d-T2CAO**, a dipolar analogue of **T2CAO**, is described in the Supporting Information.

Preparation of Organic Nanoparticles. Aqueous suspensions of organic nanoparticle were prepared according to the reprecipitation method.[69] A tetrahydrofuran (for HPLC ≥ 99.9%, from

Sigma-Aldrich) 0.5 mM stock solution of the dyes was prepared. This concentration is probably very close to the solubility limit of the compounds. 100.0 μL of solution were added to 4.90 mL of milli-Q deionized water under vigorous magnetic stirring, achieving a 1×10^{-5} M nominal concentration of the dye in the final mixture (water:THF = 98:2 v/v). The mixtures have been kept under stirring for 30 minutes, yielding clear purple (for **T1**) and orange (**T2**) suspensions. Colloidal stability was monitored spectroscopically over a few days (during that time the suspensions were stored in the dark at room temperature). DLS and zeta-potential measurements were performed at 22°C, both after a week and 20 days of aging, using a Brookhaven 90Plus/BI-MAS particle analyzer equipped with a laser source (λ_0 = 658 nm) in a 90° configuration.

Spectroscopic Measurements. Absorption and emission measurements were performed at room temperature on freshly prepared diluted solutions, to minimize self-absorption (optical density ≤ 0.1, roughly corresponding to a 10^{-6} M concentration). All solvents were spectroscopic grade (cyclohexane, AnalaR Normapur ACS purchased from VWR Chemicals; chloroform for HPLC ≥ 99.9% and dimethylsulfoxide from Sigma-Aldrich) and were used as received. For low-temperature measurements, 2-methyltetrahydrofuran (anhydrous, ≥ 99.9% from Sigma-Aldrich) was stored overnight on molecular sieves (0.3 nm) and then filtered on 2 μm PTFE filters. Absorption measurements were performed with a Perkin-Elmer Lambda 650 double-beam UV/Vis spectrophotometer. Fully corrected steady-state emission and excitation spectra were obtained with a Fluoromax-3 Horiba Jobin-Yvon fluorometer equipped with a Xenon lamp as the excitation source. We remark here a low solubility of **T2CAO** in both cyclohexane and DMSO and of **T2CAEH** in cyclohexane (A_{max} of the saturated solution << 0.1). To estimate the molar extinction coefficients in chloroform, the Lambert-Beer law was verified in the concentration range 10^{-4} - 10^{-6} M. A diluted solution ($c \sim 10^{-6}$ M) of fluorescein in NaOH(aq) 0.1 M (φ = 0.9, λ_{exc} = 460 nm) and

of cresyl violet in ethanol (φ = 0.51, λ_{exc} = 560 nm) were used as reference standards for the determination of the fluorescence quantum yields of the solutions and of the ONPs, respectively. Fluorescence decays were measured with the TCSPC (Time-Correlated Single-Photon Counting) technique, using the Fluoromax-3 instrument equipped with a Horiba Fluoro-Hub analyzer. Pulsed NanoLeds with λ = 453 or 563 nm were used as the excitation sources. The prompt signal was acquired by measuring the scattering of an aqueous suspension obtained by adding two drops of Ludox HS-40 (Sigma-Aldrich) to approximately 4 mL of water. Lifetimes (τ) values were extracted by reconvolution analysis of the decay profiles and the goodness of the fit was evaluated with the chi-square test (results were retained if $\chi^2 < 1.2$). All compounds showed a mono-exponential decay. Radiative and non-radiative rates (k_r and k_{nr}, respectively) were obtained from the experimental φ and τ values as follows:

$$k_r = \frac{\phi}{\tau}; \qquad k_{nr} = \frac{1}{\tau} - k_r$$

Anisotropy measurements were performed on vitrified 2-MeTHF solutions: under these conditions, molecular motion can be neglected. Excitation and emission anisotropies were collected with an Horiba Jobin-Yvon Fluoromax-3 instrument (single channel, L-format). The samples, contained in quartz cells especially designed for cryogenics, were rapidly cooled to 77 K (speed of cooling ~ 20°C/min) with an Oxford Instruments OptistatDN cryostat, using helium at ambient pressure as the exchange gas. Once the final temperature was reached, the system was allowed to equilibrate for 5 minutes to complete the vitrification process, yielding transparent glasses. In order to avoid sample crystallization, low concentrations of dye are required ($A_{max} \leq$ 0.05), probably because their dramatic change of solubility with temperature promotes nucleation during the cooling process. Fluorescence anisotropy r is defined as:

$$r = \frac{I_{\parallel} - I_{\perp}}{I_{\parallel} + 2I_{\perp}}$$

where $I_{\parallel}$ and $I_{\perp}$ are the emission intensities measured when the emission polarizer is oriented respectively at 0 and 90° with respect to the excitation polarizer. To compensate for the different response of the detector to light polarized in different directions, operatively *r* it is measured as:

$$r = \frac{I_{VV} - GI_{VH}}{I_{VV} + 2GI_{VH}}$$

where the subscripts *V* (for vertical) and *H* (for horizontal) refer to the orientation of the excitation (first subscript) and emission (second subscript) polarizer, respectively. The *G* factor is measured as $G = I_{HV}/I_{HH}$ as a function of the emission wavelength.

THEORETICAL MODELING

The Three-State Model. As stated above, we describe the investigated compounds as quadrupolar DAD structures, with the central acceptor (A) group corresponding to the benzothiadiazole moiety, and the donor (D) groups extending over the peripheral thiophene-cyanoacetate moieties. This suggests adopting the same ESM developed for quadrupolar CT dyes.[51] In an essential-state approach, the quadrupolar molecule is described via the resonance among three structures, taken as the basis states: the neutral $|N\rangle$ state, corresponding to the DAD state, and two degenerate zwitterionic states corresponding to the D^+A^-D and DA^-D^+ structures, $|Z_1\rangle$ and $|Z_2\rangle$, respectively. We set 2*z* as the energy gap between the neutral and the two charge-separated states. The mixing between $|N\rangle$ and each one of the zwitterionic states is $-\sqrt{2}t$, which measures the probability of electron transfer from the donors to the acceptor site. The two zwitterionic states are conveniently combined to give the symmetrized functions $|Z_+\rangle = (|Z_1\rangle + |Z_2\rangle)/\sqrt{2}$ and $|Z_-\rangle = (|Z_1\rangle - |Z_2\rangle)/\sqrt{2}$. Only $|Z_+\rangle$ mixes with the $|N\rangle$ state to yield the ground state $|g\rangle = \sqrt{1-\rho}|N\rangle +$

$\sqrt{\rho}|Z_+\rangle$ and an excited state $|e\rangle = \sqrt{\rho}|N\rangle - \sqrt{1-\rho}|Z_+\rangle$, where the ionicity ρ ($0 \leq \rho \leq 1$), corresponding to the weight of $|Z_+\rangle$ in the ground state, measures the quadrupolar character of the chromophore. $|Z_-\rangle$ remains unmixed and coincides with the lowest-energy excitation, $|c\rangle$. In V-shaped systems, as in our case, both $|c\rangle$ and $|e\rangle$ states can be reached upon linear and nonlinear absorption.[70] Since we are interested in optical spectroscopy, we must define the dipole moment operator on the chosen basis. In the simplest approximation, we neglect all matrix elements of the dipole moment operator, except μ_0, measuring the magnitude of the dipole moment associated to either $|Z_1\rangle$ or $|Z_2\rangle$, and, for V-shaped molecules, we account for the relative orientation of the two branches of the molecule, when constructing the dipole moment matrices relevant to the *x* and *y* components of the dipole moment.

A more detailed description of optical properties can be achieved introducing the coupling of the electronic degrees of freedom to molecular vibrations and polar solvation. Nuclear motion is described by means of two effective harmonic vibrational coordinates, q_1 and q_2, with frequency ω_v, associated with the relaxation of the molecular geometry along each arm as a result of the relevant CT process. The strength of the coupling is measured by the vibrational relaxation energy ε_v associated to the $|N\rangle \rightarrow |Z_{1/2}\rangle$ processes. Polar solvation is described in a reaction-field approach, treating the solvent as a continuum dielectric medium. The solvent molecules reorient around the solute producing the orientational field F_{or} which, being associated to a slow motion with respect to electronic and vibrational degrees of freedom, is treated as a classical variable. The solvation relaxation energy ε_{or} is related to the elastic restoring force of the solvent and increases with polarity (for explicit expressions see Ref.[51]). The Hamiltonian that describes the coupled electronic and vibrational motion is solved nonadiabatically. Briefly, we choose the basis obtained as the direct product of the three electronic basis states times the first *M* eigenstates of the harmonic

oscillators associated to q_1 and q_2. Diagonalization of the resulting $3M^2$-dimensional Hamiltonian gives numerically exact vibronic eigenstates, provided that M is large enough to ensure convergence. Once eigenstates are known, spectra can be calculated using relevant transition energies and dipole moments and assigning a Gaussian shape of half-width at half-maximum γ to each vibronic transition.

To account for thermal disorder, the solution is described as a collection of dyes each one experiencing a slightly different reaction field. Since the solvent coordinate is treated as an adiabatic variable, the diagonalization of the coupled electronic and vibrational Hamiltonian is repeated on a grid of F_{or} values and calculating relevant spectra. The ensemble, inhomogenously broadened, spectra are obtained as an incoherent sum of the spectra calculated for all the F_{or} values, each one weighted by its Boltzmann probability. For absorption spectra, the Boltzmann distribution is calculated based on the ground-state energy, while for emission spectra it is calculated based on the fluorescent excited state. Further details on essential-state modeling, as well as calculation of optical spectra of CT chromophores can be found in Ref. [71].

The basis states in essential-state models are diabatic states, corresponding to the main resonating structures of the dye at hand. Relevant model parameters then refer to these states, and not to the adiabatic (ground and excited) states as relevant to spectroscopy. Therefore, in essential-state models, model parameters cannot be directly related to spectral properties, but are selected to best fit experimental data (absorption and emission spectra in various solvents at room temperature). The disadvantage of losing the direct contact with observables is overcompensated by the transferability of the model parameters to describe the same dyes in different environments: indeed the same molecular model parameters are used to describe the same molecule in different solvents as well as in the aggregates.

The (non-trivial) fitting procedure is performed as follows: z and t are extracted from the position of absorption maxima, while ω_v, ε_v and γ are set to reproduce the vibronic structure, and hence the shape, of the spectra. The angle α between the two molecular arms gives the correct intensity ratio between the two absorption peaks (in the limit α = 180°, i.e. for a linear molecule, only the $|g\rangle \rightarrow |c\rangle$ transition is allowed). The dipole moment associated to the zwitterionic basis states, μ_0, is fixed to quantitatively reproduce the molar extinction coefficient in chloroform. These molecular parameters are kept fixed, independently of the solvent, and a single parameter, ε_{or}, is varied to account for solvation effects. Excitation anisotropies and low-temperature excitation spectra are obtained using the same set of parameters extracted from room temperature absorption and fluorescence spectra. In this work, low-temperature spectra as well as anisotropies have been calculated accounting for the Boltzmann distribution corresponding to 90 K, the estimated glass transition temperature of 2-MeTHF[72] (see Ref. [71] for further information on anisotropy calculation). The same parameters are used to calculate 2PA spectra as the imaginary part of the second hyperpolarizability $\mathrm{Im}\langle\gamma(-\omega;\omega,\omega,-\omega)\rangle$,[17] according to the sum-over-states expression, as detailed in Ref. [51].

Essential-State Modeling of Interacting Chromophores. To describe the optical properties of molecular aggregates, the three-state model presented above is extended to include intermolecular interactions.[57] Adopting the bottom-up modeling approach of ESMs, z and $\sqrt{2}t$ are molecular parameters independent of the surrounding environment, therefore they are the same as extracted from the analysis of the experimental transition frequencies of the solvated dyes. However, for the sake of simplicity, when modeling aggregates we neglect vibrational and solvation degrees of freedom, adopting a simplified purely electronic model, so that the effective values of the two

ESM parameters z and $\sqrt{2}t$ are slightly different from those obtained above when also taking into account the vibronic coupling.

The basis set for interacting dyes is obtained as the direct product of the 3 basis states N, Z_1 and Z_2, defined for each dye, leading to a 3^N basis, where N is the number of molecules in the aggregate. On this basis, intermolecular interactions enter the Hamiltonian as electrostatic interactions between integer point-charges located on the D (positively charged) and A (negatively charged) groups, thus affecting the energy of the basis states where at least two molecules are in a zwitterionic state. For a sketch of fundamental interactions in a dimer, see Supporting Information, Figure S1. Accordingly, the strength of the electrostatic interaction depends entirely on the distances between the D/A moieties, and hence on the geometrical parameters describing the aggregate. We only consider nearest-neighbor interaction. The diagonalization of the Hamiltonian for the aggregate yields to 3^N electronic eigenstate that are used for the calculation of optical spectra

EXPERIMENTAL RESULTS

Spectroscopic Characterization in Solution. Normalized absorption and emission spectra of the target compounds collected in different solvents are reported in Figure 2 and main spectroscopic properties are listed in Table 1. **T1CAO** and **T1CAEH** (hereafter **T1**) spectral features are similar, confirming that alkyl chains do not appreciably alter the electronic properties of dyes in solution. Absorption spectra are dominated by two electronic transitions: the most intense spans the green region of the visible spectrum (λ_{abs}^{max} ~ 500 nm), while the other is located in the UV, at λ ~ 380 nm. Other weak transitions, presumably localized on isolated functional groups, extend below 350 nm. Emission occurs above 550 nm, and is strongly affected by the solvent polarity. The vibronic structure is resolved in apolar solvents (cyclohexane), and progressively blurs upon increasing

solvent polarity, because of inhomogeneous broadening. Absorption of **T2CAO** and **T2CAEH** (**T2**) is red shifted by 30 nm with respect to the corresponding **T1** chromophores, in line with the increased conjugation length. Their spectra display a broad shape covering the 400-600 nm region, with a shoulder at approximately 450 nm. Also for the **T2** pair, the alkyl groups do not appreciably affect the spectra: replacing linear with branched chains induces only a slight red shift (~ 5 nm) of the main absorption peak with a little decrease of the intensity of the short-wavelength shoulder.

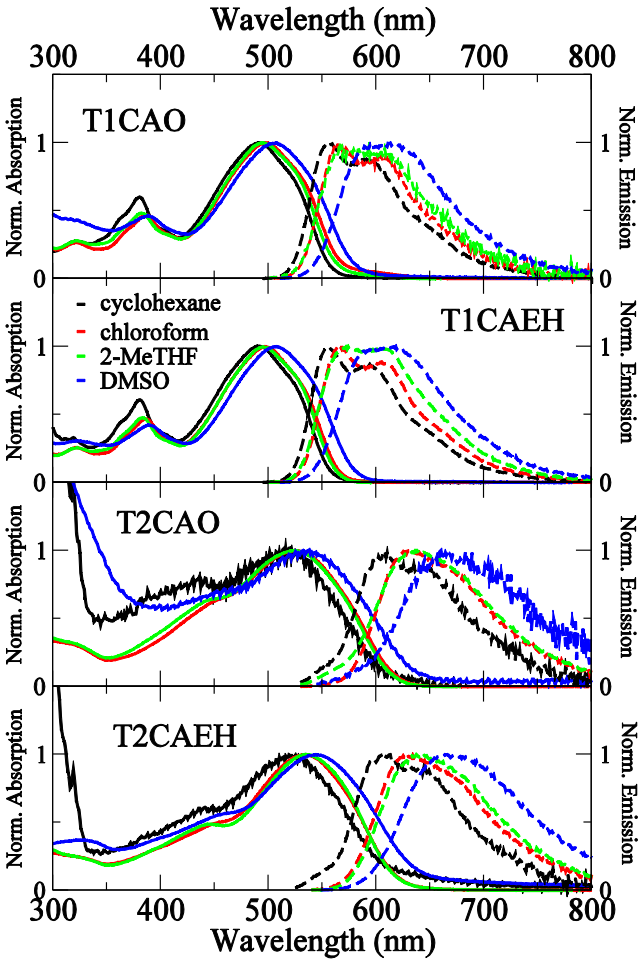

Figure 2. Experimental normalized absorption (continuous line) and emission (dashed line) spectra of the target compounds in solvents of different polarity. 2-MeTHF: 2-methyltetrahydrofuran, DMSO: dimethylsulfoxide.

Table 1. Spectroscopic Properties of the Chromophores in Solvents of Different Polarity.

compound	solvent	λ_{max}^{abs} (nm)[a]	λ_{max}^{em} (nm)	Stokes shift (cm^{-1})	ε_{max} ($M^{-1}cm^{-1}$)[b]	φ (%)[c]	τ (ns)[d]	k_r (ns^{-1})[e]	k_{nr} (ns^{-1})[f]
T1CAO	cyclohexane	490/380	556	2422		29	1.15	0.25	0.62
	chloroform	498/386	565	2381	49400	24	1.04	0.23	0.73
	2-MeTHF	495/382	566	2534		29	-[g]		
	DMSO	508/388	613	3371		22	1.21	0.18	0.64
T1CAEH	cyclohexane[h]	492/380	556	2339		28	1.17	0.24	0.61
	chloroform	497/386	564	2390	53100	26	1.05	0.25	0.70
	2-MeTHF	495/383	574	2780		31	-[g]		
	DMSO[h]	507/389	618	3542		22	1.20	0.18	0.65
T2CAO	cyclohexane[h]	520/435	608	2783		28	1.33	0.21	0.54
	chloroform	525/456	630	3175	58700	19	0.96	0.20	0.84
	2-MeTHF	525/448	638	3373		26	-[g]		
	DMSO	538/449	660	3436		17	1.19	0.14	0.70
T2CAEH	cyclohexane	519/446	610	2874		23	1.11	0.21	0.69
	chloroform	534/454	629	2828	66700	19	1.09	0.17	0.74
	2-MeTHF	534/444	644	3199		28	-[g]		
	DMSO	543/460	664	3356		17	1.09	0.15	0.76

[a] the two values refer to the main/secondary peak; [b] molar extinction coefficient at λ_{max}^{abs}; [c] fluorescence quantum yields; [d] fluorescence lifetimes; [e] radiative decay rate; [f] nonradiative decay rate; [g] not measured; [h] low solubility of the dye. 2-MeTHF: 2-methyltetrahydrofuran, DMSO: dimethylsulfoxide.

No appreciable difference between the two dyes is observed in emission. Fluorescence maxima are located between 600 and 670 nm, depending on the solvent. The vibronic structure is progressively smeared out upon increasing the solvent polarity. All compounds exhibit a weak positive solvatochromism of both absorption peaks (red shift < 20 nm from cyclohexane to DMSO) and a more pronounced emission solvatochromism ($\Delta\lambda \sim 50$ nm), suggesting the presence of a polar excited state. The chromophores display high molar extinction coefficients (50000–70000

$M^{-1}cm^{-1}$), and their fluorescence quantum yields range from 20 to 30%, being marginally affected by the solvent and the number of thiophene moieties.

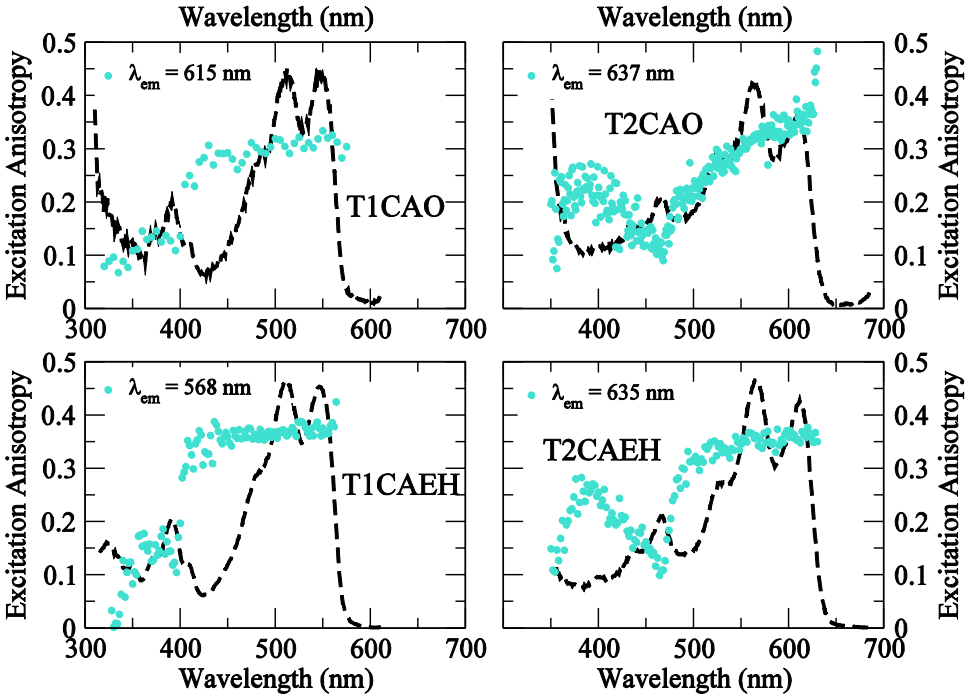

Figure 3. Excitation anisotropies (dots) of the chromophores collected in glassy 2-MeTHF matrixes at 77 K. Dashed lines show excitation spectra collected under the same experimental conditions.

Excitation anisotropies of the four dyes in glassy matrixes are shown in Figure 3. Emission anisotropies are reported in the Supporting Information (Figure S2). The alkyl chains do not affect anisotropy, any difference observed for the two dyes in each **T1** and **T2** pair being within the experimental error, and can be attributed to the formation of glasses of different quality. The investigated chromophores display similar anisotropies: *r* is almost flat and close to the maximum limiting value of 0.4 inside the main absorption peak, indicating almost parallel absorption and emission dipole moments. This is in line with the Kasha's rule, stating that emission occurs from the lowest excited singlet state, and confirms in our case the absence of trivial depolarization

processes due to molecular motion or energy transfer. Moving to shorter wavelengths, the anisotropy decreases abruptly, reaching a minimum ($r \sim 0.1$ for all systems) corresponding to the secondary absorption peak. This indicates a different polarization of the two excited states. A further increase in excitation anisotropy occurs on the blue side of the spectrum of **T2** dyes, reaching $r \sim 0.25$ at $\lambda \sim 400$ nm.

Organic Nanoparticles Suspensions. Aqueous suspensions were prepared according to the reprecipitation method. The preparation involves the rapid mixing of a concentrated solution of the dye in a suitable organic solvent with a non-solvent, typically water. The organic solvent must be fully miscible with the non-solvent, and the nanoparticles are formed by the instantaneous diffusion of the non-solvent in the solution.[73] In this work tetrahydrofuran (THF) was chosen as the organic solvent, while water plays the role of non-solvent. This simple method allowed for quick and easy preparation of stable ONPs suspensions of the four dyes. Among the systems studied in this work, **T1** dyes proved to yield the most stable suspensions, remaining clear to the naked eye with unaltered spectroscopic properties for more than one month. **T2** suspensions flocculated 20 days after preparation, even if until then no significant spectroscopic changes have been detected (for a spectroscopic proof of the colloidal stability of the suspensions see Supporting Information, Figure S3).

Morphological information is gained from Dynamic Light Scattering measurements (see Table 2 and Supporting Information). The particles span a wide dimensional range, from less than 70 nm diameter for **T1CAEH** particles to the larger **T2CAEH** aggregates of more than 300 nm diameter. **T1** compounds display similar dimensions and polydispersity (approximately 0.2), while **T2** dyes are markedly different, with the biggest particles being most polydispersed, thus indicating a subtle interplay between the side chains and molecular backbone in affecting molecular packing in the

nanoaggregates. The effect of aging is modest for **T1CAO** ONPs (~ 8 % increase of the mean diameter), while is more pronounced for **T1CAEH** suspensions (~30%), suggesting that the aggregation process continues over time leading to an increase of the particle size. The anomalous behavior of **T1CAEH** suspensions could be explained by weak repulsive interactions between particles, as pointed out by the lower absolute value of the zeta potential (~ -20 mV). According to this analysis, the other suspensions owe their stability to sizeable inter-particle electrostatic repulsions, as argued from large negative potentials (< -30 mV).

Table 2. Morphological and Spectroscopic Characterization of the ONPs.

compound	mean diameter (nm)[a,b]	polydispersity[b]	Zeta potential (mV)[b]	λ_{abs}^{max} (nm)	λ_{em}^{max} (nm)	φ (%)[c]
T1CAO	88.6	0.269	-39.87	492/565/400[d]	730	0.48 (495)
	(96.2)	(0.260)	(-35.66)			0.59 (565)
T1CAEH	67.1	0.242	-19.08	528/573/400[d]	715	1.0 (500)
	(89.0)	(0.235)	(-13.26)			1.0 (530)
						1.1 (575)
T2CAO	70.7	0.106	-31.32	484	795	0.27 (480)
						0.25 (620)
T2CAEH	325.7	0.304	-43.12	507	>800	-[e]

[a] from intensity-weighted distribution; [b] numbers in brackets refer to 20-days aged samples; [c] numbers in brackets refer to excitation wavelengths (in nm); [d] the numbers refer to absolute maximum/J-band/secondary peak; [e] the emission is too low to reliably estimate φ.

Experimental absorption and emission spectra of the suspensions are reported in Figure 4. The absorption spectrum of **T1CAO** nanoparticles consists of a broad signal centered at ~500 nm, superimposed to the main peak of the THF solution. The long-wavelength shoulder at λ ~ 565 nm is instead an exclusive feature of ONPs. **T1CAEH** shows a more complex structure of the main peak: the absolute maximum is now shifted to the red, at 530 nm, but there is still a residual signal

at λ ~ 500 nm covering the spectrum of the solution. Also in this case a prominent shoulder is present on the red side of the ONPs spectrum, at λ ~ 570 nm. For both **T1** suspensions, the secondary peak of the solution is instead red shifted by approximately 20 nm. The presence of the long-wavelength signal suggests the formation of J-aggregates for both chromophores.[74]

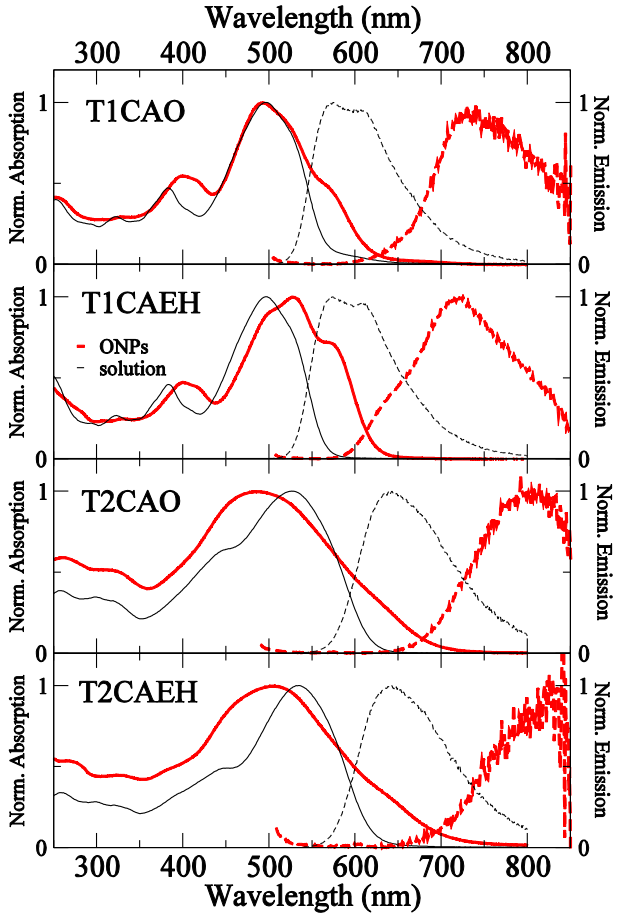

Figure 4. Experimental normalized absorption (continuous line) and emission (dashed line) spectra of ONPs suspensions (in red) and THF solutions (in black).

At variance with solution spectra, the alkyl groups largely affect the spectra of ONPs, because they govern the molecular packing, with J-aggregates being favored by branched chains, as suggested by the comparison of the corresponding absorption intensities. However, the molecules are not organized in ordered pattern and the coexistence of chromophores arranged in a disordered

way inside the same nanoparticle explains the occurrence of several overlapping signals, partially recovering solution spectra. **T2** absorption spectra reflect a larger degree of heterogeneity, resulting in a broad signal that spans a wide portion of the UV-vis spectrum. Spectral analysis for **T2** is complicated by the coalescence of the two CT bands, which could lead to the apparent blue shift of the absorption maximum. The weak shoulder at $\lambda \sim 650$ nm indicates that J-aggregated dyes represent only a small fraction of the molecules, which retain instead a mainly random arrangement. From this result, we can argue that the substitution of thiophene with the more flexible bithiophene moiety disrupts the preferentiality of packing and the peripheral chains lose their capability to direct intermolecular interactions.

Emission of the ONPs is systematically red shifted of about 150 nm with respect to solution, reaching a maximum at 730 and 715 nm for **T1CAO** and **T1CAEH**, respectively, and beyond 800 nm for **T2** suspensions. Fluorescence spectra of **T1** nanoparticles show an unusual shape, confirming the heterogeneity of the systems. In spite of the obvious presence of J-aggregates, the ONPs display an unexpectedly weak emission, with fluorescence quantum yields well below 1%, with the only exception of **T1CAEH** nanoparticles (see Table 2). Quantum yields are marginally affected by the excitation wavelength, suggesting efficient energy transfer (with a yield somewhat smaller than 100%) among the species contained inside each particle. This phenomenon is confirmed by the excitation profiles (see Supporting Information, Figure S4), that reproduce the absorption spectra. The excitation is thus transferred from non-fluorescent aggregates absorbing in the blue-side of the spectrum to the J-aggregates, which are the only ones responsible for the emission. The unusually weak emission from J-aggregates is hardly explained by the occurrence of fast nonradiative decay pathways, and claims for additional deactivation mechanisms, which will be addressed and discussed in the following section.

DISCUSSION

Theoretical Modeling in Solution. Absorption and emission spectra in Figure 5 have been calculated with the optimized parameters listed in Table 3, which have been extracted according to the fitting procedure described in the previous section.

Chromophores differing only for the alkyl chain have been modeled with the same parameters, since their experimental spectral features are substantially identical. The two sets of parameters have been extracted independently for the two pairs, **T1** and **T2**, and ensure an overall reproduction of the main experimental spectral features. Their physical meaning and comparative soundness is discussed in the SI.

A good correspondence is observed between experimental and calculated spectra, the two experimental absorption bands being unequivocally assigned to the two CT transitions characteristic of bent quadrupolar dyes.[70,75] Substitution of the thiophene with the bithiophene moiety decreases the energy difference between the two transitions, resulting in a spectral overlap of the signals. Moreover, it strongly affects the ground state charge distribution of the molecules: while the degree of charge transfer, ρ, calculated from the *z* and *t* parameters of Table 3[51], is 0.13 for **T1** dyes, it drops to 0.05 for **T2** systems, consistently with a less conjugating bridge between the donating/accepting moieties. To recover the observed experimental ratio of the two absorption peaks, a slightly more bent structure for the **T2** chromophores (110°) have been imposed, which could physically account for a longer and curved backbone.

Inhomogeneous broadening due to the increase in the solvent polarity is well accounted for. The weak absorption solvatochromism arises from the V-shaped structure of the chromophores, responsible for a non-zero ground state dipole moment,[70] and is effectively described by the model. Emission solvatochromism is explained, according to the model, by a symmetry breaking in the

excited state: emission occurs from a polar state where the excitation is localized on one molecular arm. This behavior is typical of class I quadrupolar chromophores, characterized by a largely neutral ground state.[51]

Table 3. Essential-State Parameters Adopted for the Calculation of Optical Spectra.

	T1	**T2**
z (eV)	1.02	1.14
$\sqrt{2}t$ (eV)	0.96	0.58
ω_v (eV)	0.17	0.20
ε_v (eV)	0.53	0.39
γ (eV)	0.07	0.08
μ_0 (D)	22.0	36.5
α (°)	120	110

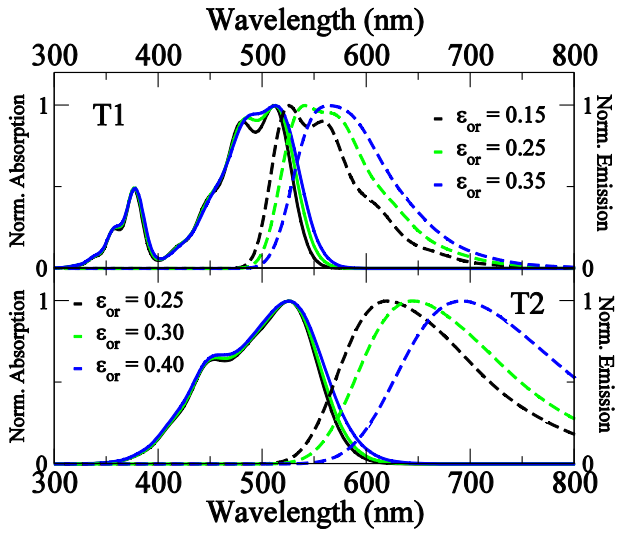

Figure 5. Calculated absorption (continuous line) and emission (dashed line) spectra of the target compounds in solvents of different polarity. The relevant parameters are listed in Table 3. ε_{or} values (in eV) corresponding to the various solvents are reported on the panels (black: cyclohexane, green: 2-MeTHF, blue: DMSO).

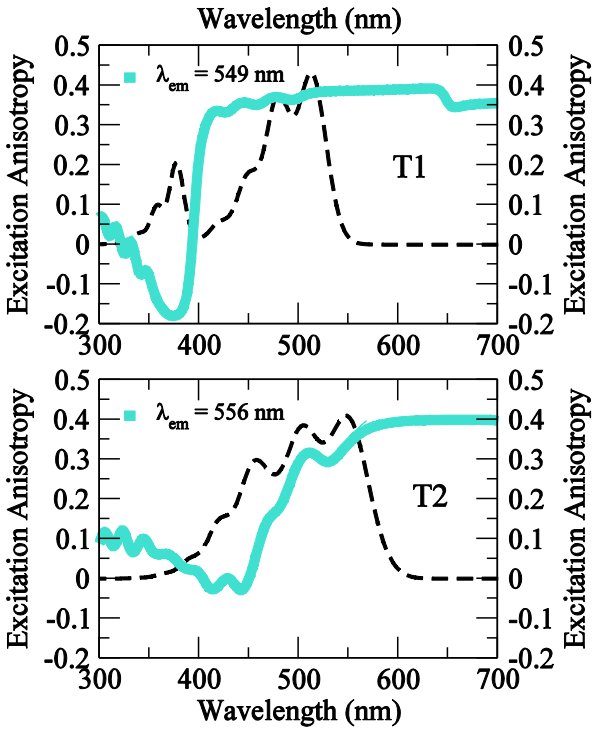

Figure 6. Calculated excitation anisotropies (blue lines) and excitation spectra (dashed lines) with the parameters of Table 3 (ε_{or} = 0.25 for **T1** and 0.30 for **T2**).

Qualitative comparison of the experimental and calculated anisotropies (Figure 6 and Figure S5) confirms the ability of the model to capture the low energy physics of these systems. The sudden change of *r* from the maximum 0.4 to the minimum ~-0.2 limiting value in the region between the two CT transitions stems from the fact that in a prototypical V-shaped chromophore the two transitions are mutually perpendicular, with the highest energy one being aligned along the C_2 axis.[70] This behavior is qualitatively in line with the experimental one, with the deviations from the lowest anisotropy value (experimental ~0.1 versus calculated -0.2) being ascribed to spectral overlap of the secondary peak with localized transitions. The quadrupolar character of the chromophores is further emphasized by comparison with the experimental properties of the dipolar

(DA) analogue of **T2CAO**. In this case, only one peak is observed in absorption corresponding to its unique CT transition (see Supporting Information, Figures S6, S7 and Table S1).[48]

Having validated the model against experimental data, we can use this tool to anticipate other optical properties of interest of the investigated compounds, such as 2PA spectra (Figure S8). For both systems we predict a 2PA response close to 1500 GM (neglecting any local field correction; 1GM = 10^{-50}cm^4·s·photons^{-1}). **T1** response comes in a sharp band located in the red region ($\lambda \sim$ 750 nm) with a tail above 800 nm, reproducing the spectral shape of the OPA (One-Photon Absorption) spectrum. Conversely, **T2** absorption is broad and covers a much wider spectral range (800 – 1200 nm), partially overlapping the biological transparency window, suggesting potential applications also in biological field for imaging purposes.

Theoretical Modeling of Aggregates. Molecular aggregates are usually classified on the basis of the position of their absorption maximum with respect to the monomer in solution. A blue-shift of the absorption peak denotes an H-aggregate, while a red-shift indicates a J-aggregate. According to the exciton model, H-aggregates experience complete quenching of fluorescence, since their lowest-energy excited state possesses a vanishing transition dipole moment. J-aggregates are instead expected to be strongly fluorescent, being the maximum oscillator strength associated to the transition towards the lowest excited state.[76]

As seen from the experimental spectra of ONPs, **T1** dyes arrange in a partly ordered structure forming stable J-aggregates, as demonstrated by the presence of a new, red-shifted absorption band not present in the solution. However, the low fluorescence contrasts with the exciton picture. Here we demonstrate that ESMs can naturally explain this anomalous behavior. In the following, we will focus only on the description of **T1** aggregates, since the high degree of disorder that characterizes **T2** ONPs hinders the interpretation of experimental data.

In our approach, only intermolecular electrostatic interactions are considered, disregarding any possible intermolecular charge-transfer interaction. In fact, in this specific case, the molecules bear long side chains and the aggregated structures are kinetics-driven, so that very close spacing between the molecules, short enough to ensure significant overlap of the molecular orbitals, is unlikely. For this same reason, an intermolecular CT band would be expected at much lower energy (down in the red or NIR spectral region), with negligible oscillator strength.

According to ESMs, the spectral shifts are governed by the interplay of two effects. The first, is similar to the one described in the typical exciton theory and mainly arises from the orientation of the transition dipole moments of the interacting molecules. The second contribution is a mean-field effect, completely overlooked in the exciton model, arising from the electrostatic interaction between one molecule and the electrostatic potential generated by the neighboring ones; this contribution becomes particularly relevant for highly polarizable molecules[59,60,64]. This could be either a stabilizing (mainly attractive interactions) or a destabilizing (predominance of repulsions) effect, contributing to a red or a blue shift, respectively.[60]

For the sake of simplicity, we will address at the beginning a molecular dimer, in an edge-to-edge geometry, with both molecules in the same plane, as sketched in Figure 7. The first one is placed with the acceptor moiety on the origin of the Cartesian axes and the two donor groups pointing towards the positive y direction. The second molecule is translated of s_y = 8 Å along y, which is equivalent to impose a distance of 4.5 Å between the D moiety of the upper molecule and the A moiety of the lower molecule, when they are aligned. We have imposed a molecular arm length l of 7 Å. This choice is arbitrary, since no structural data are available for the target compounds, however the values assigned to the geometrical parameters are of the same order of magnitude of those already adopted in the essential-state modeling of similar systems.[64] The angle

α between the molecular arms is instead fixed according to the modeling in solution previously described. The effect of the geometry on the optical properties of the aggregate is studied by keeping the first molecule in a fixed position and displacing the second of s_x along the x axis, as shown in the figure. In Figure 8, we report for each s_x value (from 0 to 14 Å, by steps of 1 Å) the transition energies from the ground state to the first four excited states calculated for a **T1** dimer. As already underlined elsewhere, only these four states are relevant for the description of low-energy spectroscopy of the aggregates.[64]

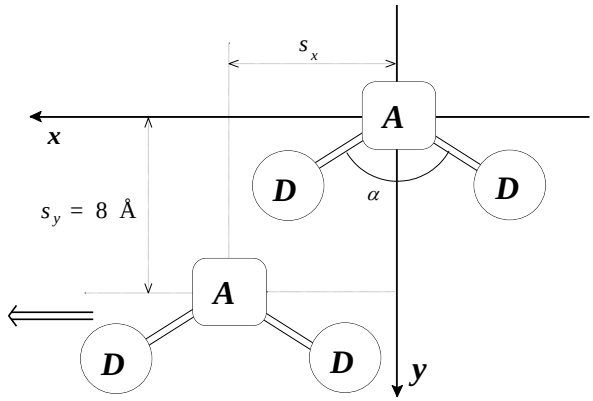

Figure 7. Geometrical description of the dimer in the essential-state modelling. One molecule is kept fixed, while the other is translated in the direction indicated by the bold arrow.

For each geometry, only two electronic transitions display sizeable oscillator strengths. The highest-energy transition is the least intense and always experiences a red shift, independently of s_x. Concerning the lowest-energy transition, relevant to the description of fluorescence, we have that for $s_x < 3$ Å, the transition energy of the dimer is always higher than the corresponding energy of the monomer: therefore, we expect a blue-shift of the absorption peak with respect to the isolated molecule, denoting an H-aggregate. For further increases in s_x, the transition energy of the dimer is always below the one of the monomer, so that we expect a red-shift of the dimer absorption band, denoting a J-aggregate. The oscillator strength associated with the lowest energy transition

increases from zero (complete quenching of fluorescence) at small s_x, towards to ~ 0.17 for $s_x \geq 10$ Å (spontaneous emission fully allowed). From 6 to 8 Å the transition to the second excited-state still dominates the absorption spectrum, but a non-vanishing yet very small oscillator strength is calculated for the lowest-energy band, making the fluorescence emission not completely forbidden.

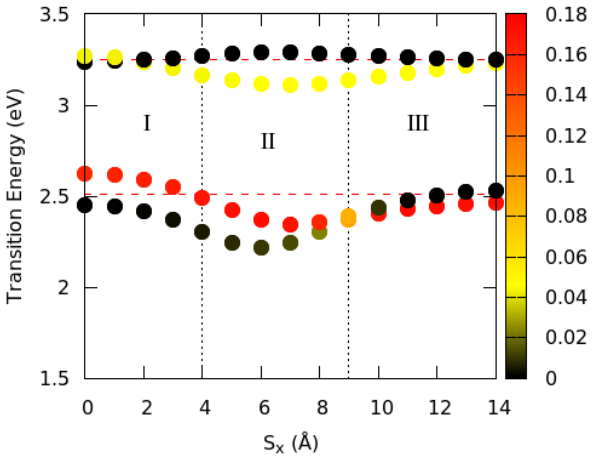

Figure 8. Energies of the four lowest excited states of a **T1** dimer versus the geometrical parameter s_x, calculated according to the three-state model (the values are all relative to the ground state, which is assumed as the zero of the energy; the shift s_y has been fixed to 8 Å). The palette indicates the oscillator strengths of the transitions. Horizontal red lines refer to the two transition energies calculated for the monomer (2.51 and 3.25 eV). The three regions correspond to different spectroscopic behavior, as described in the text: I, standard (non-fluorescent) H-aggregates; II, non-fluorescent J-aggregates; III, standard (fluorescent) J-aggregates. Model parameters: z = 0.89 eV, $\sqrt{2}t$ = 0.96 eV, α = 120°.

Combining these observations, three different regions can be defined, depending on the geometric shift s_x. In the first region, (indicated on the graph as I) a blue-shift of the absorption maximum is expected, together with a loss of fluorescence: this is the typical case of H-aggregates. For a shift higher than 8 Å (region III), we expect a red-shift of the absorption band together with

spontaneous emission, as usual for J-aggregates. In the central region (II), roughly between 3 and 8 Å, a bathochromic shift of the main absorption peak is expected, as typical for J-aggregates, but the "fluorescent" state has small or vanishing transition dipole moment, leading to a dramatic reduction or even complete quenching of the emission. Aggregates falling into this region have no counterpart in the classical exciton picture, but their unusual behavior is naturally explained in the essential-state approach by the occurrence of a low-energy dark state. It is worth noticing that the largest red-shifts of the main absorption peak are expected in this region (the maximum calculated shift is > 30 nm), as a consequence of the high electrostatic stabilization of states occurring when the oppositely charged groups are in close proximity, and are consistent with experimental result.

We stress here that the obtained results contrast with predictions based on the exciton model. In fact, even for a dimer, we expect more than two excited states to be located at energy similar to the monomer's excited state (see Figure 8), so that a few different scenarios (not predicted by the exciton picture) are possible, well beyond the standard J or H-aggregate scheme. In particular, for our "non-fluorescent J-aggregates" (region II), most of the oscillator strength is associated to a state that is *red-shifted* with respect to the monomer (hence the appellation "J") but another, even more red-shifted state is found that, having a negligible oscillator strength, explains the observed suppression of fluorescence.

The same calculation has been performed on the same dimer for different values of shift s_y (Figure S9), obtaining qualitatively similar results: the three regions can always be recognized, even if in slightly different locations. This gives confidence on the reliability of the results for dimers having the geometry type sketched in Figure 7.

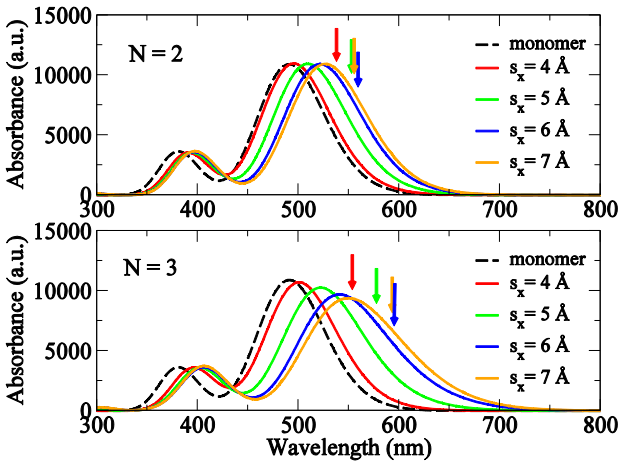

Figure 9. Calculated absorption spectra of aggregates belonging to region II for **T1** dimer (N=2) and trimer (N=3), according to the model. Dashed lines refer to the absorption spectrum of the monomer. Spectra have been obtained assigning to each transition a Gaussian bandshape with half-width at half-maximum γ = 0.2 eV and intensities have been renormalized for the number of molecules. Arrows indicate the position of the dark state.

The same qualitative considerations also apply to trimers of **T1**, obtained aligning one more molecule with the others, thus forming a monodimensional molecular ladder. The calculated absorption spectra of non-fluorescent J-dimers and trimers of **T1** are shown in Figure 9. Increasing the dimension from N=2 to N=3 mainly results in higher red-shifts of the main absorption peak, up to 50 nm, while the first excited state is once again dark, confirming the quenching of fluorescence also for the trimer. With this simple model, we are able to simultaneously account for the large experimental red-shifts observed in both absorption and emission spectra and for the low fluorescence quantum yields of ONPs of **T1**. On the basis of purely spectroscopic observations, we can therefore locate **T1** aggregates in region II of Figure 8. At this stage, the proposed edge-to-edge arrangement of the dyes cannot be confirmed due to the lack of structural data. However, a literature survey suggests that, while it is fairly common for quasi-planar small conjugated molecules to crystallize with a face-to-face arrangement of the molecular units to form

unidirectional π-π stacks,[77] it is also well known that the benzothiadiazole building block is able to promote the formation, through directional intermolecular N···S contacts, of more complex and extended self-assembled architectures, depending on the nature of the substituents.[78] These include herringbone patterns arranged in tape-like planar structures, where the molecules are slipped along one direction.[79] Moreover, reprecipitation implies that ONPs form under kinetic control, and other thermodynamically less favored molecular packings cannot be excluded. This give us confidence on the plausibility of the proposed arrangement of the dyes in the nanoaggregates. In this direction, however, further structure elucidation is in progress.

CONCLUSIONS

Four charge-transfer chromophores containing the electron accepting benzothiadiazole and two electron-donating thiophene (or bithiophene) units have been spectroscopically characterized in solution. Thanks to their V-shaped structure, their absorption spectra display two CT transitions covering a large portion of the UV/vis spectrum, thus making them of potential interest in solar light harvesting systems. The dyes yield stable suspensions of nanoparticles in aqueous media, obtained via the classical reprecipitation method. In spite of being an easy and straightforward technique for the preparation of nanosuspensions, the main drawback of reprecipitation is the lack of control on the particle formation process, resulting in a variable morphology and heterogeneous molecular packing. However, we have strong spectroscopic evidence of the formation of J-aggregates, to a certain extent governed by the terminal alkyl chains. The spectroscopic study of the suspensions reveals unexpectedly low fluorescence quantum yields that cannot be explained within the classical exciton theory. This anomalous result is rationalized based on an ESM approach to aggregates that fully accounts for the molecular polarizability. A three-state model for quadrupolar dyes is first parameterized and validated against spectral properties of solvated dyes.

The model reproduces well linear absorption and fluorescence spectra of the target compounds in solution, as well as their anisotropy spectra in glassy matrices. We predict for **T2**-dyes a good 2PA response in the red-NIR region, making them suitable candidates for bioimaging purposes. Finally, the three-state model has been implemented for the description of interacting chromophores, introducing electrostatic interactions. For the special case of dimers and trimers of quadrupolar chromophores arranged in a ladder geometry, three different spectroscopic behaviors are predicted depending on the lateral shift of the dyes. Besides standard H- and J-aggregates based on the exciton picture, and any "intermediate" aggregated form, we discussed here the occurrence of qualitatively different types of assemblies, not envisaged in the exciton picture. For these aggregates we predict large red-shifts of the absorption peak together with fluorescence quenching, thanks to the presence of a dark state with lower energy with respect to the state populated in absorption, making sense of the experimental spectroscopic behavior.

ASSOCIATED CONTENT

Supporting Information. The Supporting Information is available free of charge at … Synthesis of **d-T2CAO**; sketch of intermolecular interactions assumed in the theoretical modeling; experimental emission anisotropies; stability and fluorescence excitation spectra of ONPs; discussion about the values of molecular parameters; DLS and Z-potential data; calculated emission anisotropies; spectroscopic characterization of **d-T2CAO**; calculated two-photon absorption spectra; transition energies calculated for dimers with different geometries.

ACKNOWLEDGMENT

The authors gratefully acknowledge financial support from China Scholarship Council and from the Italian Ministero dell'Istruzione, dell'Università e della Ricerca (program FIRB "Futuro in Ricerca 2010" grant RBFR10Y5VW and program PRIN grant 2012T9XHH7).

REFERENCES

(1) Bureš, F. Fundamental Aspects of Property Tuning in Push–pull Molecules. *RSC Adv.* **2014**, *4*, 58826–58851.

(2) Kim, T.; Lee, K. D- π -A Conjugated Molecules for Optoelectronic Applications. *Macromol. Rapid Commun.* **2015**, *36*, 943–958.

(3) Slama-Schwok, A.; Blanchard-Desce, M.; Lehn, J.-M. Intramolecular Charge Transfer in Donor-Acceptor Molecules. *J. Phys. Chem.* **1990**, *94*, 3894–3902.

(4) Zhu, H.; Wang, X.; Ma, R.; Kuang, Z.; Guo, Q.; Xia, A. Intramolecular Charge Transfer and Solvation of Photoactive Molecules with Conjugated Push-Pull Structures. *ChemPhysChem* **2016**, *17*, 3245–3251.

(5) Bureš, F.; Bernd Schweizer, W.; May, J. C.; Boudon, C.; Gisselbrecht, J. P.; Gross, M.; Biaggio, I.; Diederich, F. Property Tuning in Charge-Transfer Chromophores by Systematic Modulation of the Spacer between Donor and Acceptor. *Chem. - A Eur. J.* **2007**, *13*, 5378–5387.

(6) Koch, N. Organic Electronic Devices and Their Functional Interfaces. *ChemPhysChem* **2007**, *8*, 1438–1455.

(7) Bulović, V.; Shoustikov, A.; Baldo, M. A.; Bose, E.; Kozlov, V. G.; Thompson, M. E.; Forrest, S. R. Bright, Saturated, Red-to-Yellow Organic Light-Emitting Devices Based on

Polarization-Induced Spectral Shifts. *Chem. Phys. Lett.* **1998**, *287*, 455–460.

(8) Qian, G.; Zhong, Z.; Luo, M.; Yu, D.; Zhang, Z.; Wang, Z. Y.; Ma, D. Simple and Efficient near-Infrared Organic Chromophores for Light-Emitting Diodes with Single Electroluminescent Emission above 1000 nm. *Adv. Mater.* **2009**, *21*, 111–116.

(9) Cho, N.; Kim, J.; Song, K.; Lee, J. K.; Ko, J. Synthesis and Characterization of Push-Pull Organic Semiconductors with Various Acceptors for Solution-Processed Small Molecule Organic Solar Cells. *Tetrahedron* **2012**, *68*, 4029–4036.

(10) Sim, J.; Do, K.; Song, K.; Sharma, A.; Biswas, S.; Sharma, G. D.; Ko, J. D-A-D-A-D Push Pull Organic Small Molecules Based on 5,10-dihydroindolo[3,2-B]indole (DINI) Central Core Donor for Solution Processed Bulk Heterojunction Solar Cells. *Org. Electron.* **2016**, *30*, 122–130.

(11) Castro, E.; Cabrera-Espinoza, A.; Deemer, E.; Echegoyen, L. Low-Energy-Gap Organic Based Acceptor-Donor-Acceptor π-Conjugated Small Molecules for Bulk-Heterojunction Organic Solar Cells. *European J. Org. Chem.* **2015**, *2015*, 4629–4634.

(12) Li, Y.; Hu, J.; He, G.; Zhu, H.; Wang, X.; Guo, Q.; Xia, A.; Lin, Y.; Wang, J.; Zhan, X. Influence of Thiophene Moiety on the Excited State Properties of Push-Pull Chromophores. *J. Phys. Chem. C* **2016**, *120*, 13922–13930.

(13) Neto, B. A. D.; Lapis, A. A. M.; Da Silva Jùnior, E. N.; Dupont, J. 2,1,3-Benzothiadiazole and Derivatives: Synthesis, Properties, Reactions, and Applications in Light Technology of Small Molecules. *European J. Org. Chem.* **2013**, 228–255.

(14) Duan, C.; Li, J.; Han, C.; Ding, D.; Yang, H.; Wei, Y.; Xu, H. Multi-Dipolar Chromophores

Featuring Phosphine Oxide as Joint Acceptor: A New Strategy toward High-Efficiency Blue Thermally Activated Delayed Fluorescence Dyes. *Chem. Mater.* **2016**, *28*, 5667–5679.

(15) Sonar, P.; Singh, S. P.; Leclère, P.; Surin, M.; Lazzaroni, R.; Lin, T. T.; Dodabalapur, A.; Sellinger, A. Synthesis, Characterization and Comparative Study of Thiophene–benzothiadiazole Based Donor–acceptor–donor (D–A–D) Materials. *J. Mater. Chem.* **2009**, *19*, 3228–3237.

(16) Mori, T. Organic Charge-Transfer Salts and the Component Molecules in Organic Transistors. *Chem. Lett.* **2011**, *40*, 428–434.

(17) Terenziani, F.; Katan, C.; Badaeva, E.; Tretiak, S.; Blanchard-Desce, M. Enhanced Two-Photon Absorption of Organic Chromophores: Theoretical and Experimental Assessments. *Adv. Mater.* **2008**, *20*, 4641–4678.

(18) Susumu, K.; Fisher, J. A. N.; Zheng, J.; Beratan, D. N.; Yodh, A. G.; Therien, M. J. Two-Photon Absorption Properties of Proquinoidal D-A-D and A-D-A Quadrupolar Chromophores. *J. Phys. Chem. A* **2011**, *115*, 5525–5539.

(19) Beljonne, D.; Wenseleers, W.; Zojer, E.; Shuai, Z.; Vogel, H.; Pond, S. J. K.; Perry, J. W.; Marder, S. R.; Brédas, J. L. Role of Dimensionality on the Two-Photon Absorption Response of Conjugated Molecules: The Case of Octupolar Compounds. *Adv. Funct. Mater.* **2002**, *12*, 631–641.

(20) He, G. S.; Tan, L.-S.; Zheng, Q.; Prasad, P. N. Multiphoton Absorbing Materials : Molecular Designs , Characterizations , and Applications. *Chem. Rev.* **2008**, *108*, 1245–1330.

(21) Rouxel, C.; Charlot, M.; Mir, Y.; Frochot, C.; Mongin, O.; Blanchard-Desce, M. Banana-

Shaped Biphotonic Quadrupolar Chromophores: From Fluorophores to Biphotonic Photosensitizers. *New J. Chem.* **2011**, *35*, 1771–1780.

(22) Velusamy, M.; Shen, J. Y.; Lin, J. T.; Lin, Y. C.; Hsieh, C. C.; Lai, C. H.; Lai, C. W.; Ho, M. L.; Chen, Y. C.; Chou, P. T.; et al. A New Series of Quadrupolar Type Two-Photon Absorption Chromophores Bearing 11, 12-Dibutoxydibenzo[a,c]-Phenazine Bridged Amines; Their Applications in Two-Photon Fluorescence Imaging and Two-Photon Photodynamic Therapy. *Adv. Funct. Mater.* **2009**, *19*, 2388–2397.

(23) Horn, D.; Rieger, J. Organic Nanoparticles in the Aqueous Phase-Theory, Experiment, and Use. *Angew. Chem. Int. Ed. Engl.* **2001**, *40*, 4330–4361.

(24) Schill, J.; Schenning, A. P. H. J.; Brunsveld, L. Self-Assembled Fluorescent Nanoparticles from π-Conjugated Small Molecules: En Route to Biological Applications. *Macromol. Rapid Commun.* **2015**, *36*, 1306–1321.

(25) McDonald, T. O.; Martin, P.; Patterson, J. P.; Smith, D.; Giardiello, M.; Marcello, M.; See, V.; O'Reilly, R. K.; Owen, A.; Rannard, S. Multicomponent Organic Nanoparticles for Fluorescence Studies in Biological Systems. *Adv. Funct. Mater.* **2012**, *22*, 2469–2478.

(26) Omer, K. M.; Ku, S.-Y.; Cheng, J.-Z.; Chou, S.-H.; Wong, K.-T.; Bard, A. J. Electrochemistry and Electrogenerated Chemiluminescence of a Spirobifluorene-Based Donor (Triphenylamine) - Acceptor (2 , 1 , 3-Benzothiadiazole) Molecule and Its Organic Nanoparticles. *J. Am. Chem. Soc.* **2011**, *133*, 5492–5499.

(27) Ishi-i, T.; Kitahara, I.; Yamada, S.; Sanada, Y.; Sakurai, K.; Tanaka, A.; Hasebe, N.; Yoshihara, T.; Tobita, S. Amphiphilic Benzothiadiazole-Triphenylamine-Based

Aggregates That Emit Red Light in Water. *Org. Biomol. Chem.* **2015**, *13*, 1818–1828.

(28) Mei, J.; Hong, Y.; Lam, J. W. Y.; Qin, A.; Tang, Y.; Tang, B. Z. Aggregation-Induced Emission: The Whole Is More Brilliant than the Parts. *Adv. Mater.* **2014**, *26*, 5429–5479.

(29) Hong, Y.; Lam, J. W. Y.; Tang, B. Z. Aggregation-Induced Emission. *Chem. Soc. Rev.* **2011**, *40*, 5361–5388.

(30) Campioli, E.; Nikolaidou, D. M.; Hugues, V.; Campanini, M.; Nasi, L.; Blanchard-Desce, M.; Terenziani, F. Amplified Two-Photon Brightness in Organic Multicomponent Nanoparticles. *J. Mater. Chem. C* **2015**, *3*, 7483–7491.

(31) Shi, X.; Xu, Z.; Liao, Q.; Wu, Y.; Gu, Z.; Zheng, R.; Fu, H. Aggregation Enhanced Two-Photon Fluorescence of Organic Nanoparticles. *Dye. Pigment.* **2015**, *115*, 211–217.

(32) D'Aléo, A.; Felouat, A.; Heresanu, V.; Ranguis, A.; Chaudanson, D.; Karapetyan, A.; Giorgi, M.; Fages, F. Two-Photon Excited Fluorescence of BF_2 Complexes of Curcumin Analogues: Toward NIR-to-NIR Fluorescent Organic Nanoparticles. *J. Mater. Chem. C* **2014**, *2*, 5208–5215.

(33) Parthasarathy, V.; Fery-Forgues, S.; Campioli, E.; Recher, G.; Terenziani, F.; Blanchard-Desce, M. Dipolar versus Octupolar Triphenylamine-Based Fluorescent Organic Nanoparticles as Brilliant One- and Two-Photon Emitters for (Bio)imaging. *Small* **2011**, *7*, 3219–3229.

(34) Zhang, J.; Chen, R.; Zhu, Z.; Adachi, C.; Zhang, X.; Lee, C. S. Highly Stable Near-Infrared Fluorescent Organic Nanoparticles with a Large Stokes Shift for Noninvasive Long-Term Cellular Imaging. *ACS Appl. Mater. Interfaces* **2015**, *7*, 26266–26274.

(35) Weissleder, R.; Nahrendorf, M.; Pittet, M. J. Imaging Macrophages with Nanoparticles. *Nat. Mater.* **2014**, *13*, 125–138.

(36) Wolfbeis, O. S. An Overview of Nanoparticles Commonly Used in Fluorescent Bioimaging. *Chem. Soc. Rev.* **2015**, *44*, 4743–4768.

(37) Fischer, I.; Petkau-Milroy, K.; Dorland, Y. L.; Schenning, A. P. H. J.; Brunsveld, L. Self-Assembled Fluorescent Organic Nanoparticles for Live-Cell Imaging. *Chem. - A Eur. J.* **2013**, *19*, 16646–16650.

(38) Yu, J.; Zhang, X.; Hao, X.; Zhang, X.; Zhou, M.; Lee, C. S.; Chen, X. Near-Infrared Fluorescence Imaging Using Organic Dye Nanoparticles. *Biomaterials* **2014**, *35*, 3356–3364.

(39) Würthner, F.; Kaiser, T. E.; Saha-Möller, C. R. J-Aggregates: From Serendipitous Discovery to Supramolecular Engineering of Functional Dye Materials. *Angew. Chemie - Int. Ed.* **2011**, *50*, 3376–3410.

(40) Hestand, N. J.; Spano, F. C. Molecular Aggregate Photophysics beyond the Kasha Model: Novel Design Principles for Organic Materials. *Acc. Chem. Res.* **2017**, 341–350.

(41) Li, Y.; Liu, T.; Liu, H.; Tian, M. Z.; Li, Y. Self-Assembly of Intramolecular Charge-Transfer Compounds into Functional Molecular Systems. *Acc. Chem. Res.* **2014**, *47*, 1186–1198.

(42) Storhoff, J. J.; Mucic, R. C.; Mirkin, C. A. Strategies for Organizing Nanoparticles into Aggregate Structures and Functional Materials. *J. Clust. Sci.* **1997**, *8*, 179–216.

(43) Deing, K. C.; Mayerhöffer, U.; Würthner, F.; Meerholz, K. Aggregation-Dependent

Photovoltaic Properties of squaraine/PC61BM Bulk Heterojunctions. *Phys. Chem. Chem. Phys.* **2012**, *14*, 8328–8334.

(44) Barzoukas, M.; Blanchard-Desce, M. Figures of Merit of Push-Pull Molecules in Photorefractive Polymers. *J Chem Phys* **2000**, *112*, 2036–2044.

(45) Barzoukas, M.; Blanchard-Desce, M. Molecular Engineering of Push–pull Dipolar and Quadrupolar Molecules for Two-Photon Absorption: A Multivalence-Bond States Approach. *J. Chem. Phys.* **2000**, *113*, 3951–3959.

(46) Ventelon, L.; Moreaux, L.; Mertz, J.; Blanchard-Desce, M. Optimization of Quadrupolar Chromophores for Molecular Two-Photon Absorption. *Synth. Met.* **2002**, *127*, 17–21.

(47) Grisanti, L.; Sissa, C.; Terenziani, F.; Painelli, A.; Roberto, D.; Tessore, F.; Ugo, R.; Quici, S.; Fortunati, I.; Garbin, E.; et al. Enhancing the Efficiency of Two-Photon Absorption by Metal Coordination. *Phys. Chem. Chem. Phys.* **2009**, *11*, 9450–9457.

(48) Sissa, C.; Parthasarathy, V.; Drouin-Kucma, D.; Werts, M. H. V; Blanchard-Desce, M.; Terenziani, F. The Effectiveness of Essential-State Models in the Description of Optical Properties of Branched Push-Pull Chromophores. *Phys. Chem. Chem. Phys.* **2010**, *12*, 11715–11727.

(49) Terenziani, F.; D'Avino, G.; Painelli, A. Multichromophores for Nonlinear Optics: Designing the Material Properties by Electrostatic Interactions. *ChemPhysChem* **2007**, *8*, 2433–2444.

(50) Boldrini, B.; Cavalli, E.; Painelli, A.; Terenziani, F. Polar Dyes in Solution: A Joint Experimental and Theoretical Study of Absorption and Emission Band Shapes. *J. Phys.*

Chem. A **2002**, *106*, 6286–6294.

(51) Terenziani, F.; Painelli, A.; Katan, C.; Charlot, M.; Blanchard-Desce, M. Charge Instability in Quadrupolar Chromophores: Symmetry Breaking and Solvatochromism. *J. Am. Chem. Soc.* **2006**, *128*, 15742–15755.

(52) Terenziani, F.; Sissa, C.; Painelli, A. Symmetry Breaking in Octupolar Chromophores: Solvatochromism and Electroabsorption. *J. Phys. Chem. B* **2008**, *112*, 5079–5087.

(53) Painelli, A.; Terenziani, F. A Non-Perturbative Approach to Solvatochromic Shifts of Push–pull Chromophores. *Chem. Phys. Lett.* **1999**, *312*, 211–220.

(54) Terenziani, F.; Przhonska, O. V.; Webster, S.; Padilha, L. A.; Slominsky, Y. L.; Davydenko, I. G.; Gerasov, A. O.; Kovtun, Y. P.; Shandura, M. P.; Kachkovski, A. D.; et al. Essential-State Model for Polymethine Dyes: Symmetry Breaking and Optical Spectra. *J. Phys. Chem. Lett.* **2010**, *1*, 1800–1804.

(55) Hu, H.; Przhonska, O. V.; Terenziani, F.; Painelli, A.; Fishman, D.; Ensley, T. R.; Reichert, M.; Webster, S.; Bricks, J. L.; Kachkovski, A. D.; et al. Two-Photon Absorption Spectra of a near-Infrared 2-Azaazulene Polymethine Dye: Solvation and Ground-State Symmetry Breaking. *Phys. Chem. Chem. Phys.* **2013**, *15*, 7666–7678.

(56) Terenziani, F.; Parthasarathy, V.; Pla-Quintana, A.; Maishal, T.; Caminade, A. M.; Majoral, J. P.; Blanchard-Desce, M. Cooperative Two-Photon Absorption Enhancement by through-Space Interactions in Multichromophoric Compounds. *Angew. Chemie - Int. Ed.* **2009**, *48*, 8691–8694.

(57) Sissa, C.; Terenziani, F.; Painelli, A.; Abbotto, A.; Bellotto, L.; Marinzi, C.; Garbin, E.;

Ferrante, C.; Bozio, R. Dimers of Quadrupolar Chromophores in Solution: Electrostatic Interactions and Optical Spectra. *J. Phys. Chem. B* **2010**, *114*, 882–893.

(58) Todescato, F.; Fortunati, I.; Carlotto, S.; Ferrante, C.; Grisanti, L.; Sissa, C.; Painelli, A.; Colombo, A.; Dragonetti, C.; Roberto, D. Dimers of Polar Chromophores in Solution: Role of Excitonic Interactions in One- and Two-Photon Absorption Properties. *Phys. Chem. Chem. Phys.* **2011**, *13*, 11099–11109.

(59) Painelli, A.; Terenziani, F. Multielectron Transfer in Clusters of Polar-Polarizable Chromophores. *J. Am. Chem. Soc.* **2003**, *125*, 5624–5625.

(60) Terenziani, F.; Painelli, A. Supramolecular Interactions in Clusters of Polar and Polarizable Molecules. *Phys. Rev. B* **2003**, *68*, 165405–165413.

(61) Terenziani, F.; Painelli, A. Collective and Cooperative Phenomena in Molecular Materials: Dimers of Polar Chromophores. *J. Lumin.* **2005**, *112*, 474–478.

(62) Datta, A.; Terenziani, F.; Painelli, A. Cooperative Interactions in Supramolecular Aggregates: Linear and Nonlinear Responses in calix[4]arenes. *ChemPhysChem* **2006**, *7*, 2168–2174.

(63) D'Avino, G.; Terenziani, F.; Painelli, A. Aggregates of Quadrupolar Dyes: Giant Two-Photon Absorption from Biexciton States. *J. Phys. Chem. B* **2006**, *110*, 25590–25592.

(64) Sanyal, S.; Painelli, A.; Pati, S. K.; Terenziani, F.; Sissa, C. Aggregates of Quadrupolar Dyes for Two-Photon Absorption: The Role of Intermolecular Interactions. *Phys. Chem. Chem. Phys.* **2016**, *18*, 28198–28208.

(65) Wang, C.; Cao, Z.; Zhao, B.; Shen, P.; Liu, X.; Li, H.; Shen, T.; Tan, S. Synthesis and

Photovoltaic Properties of Organic Small Molecules Containing Triphenylamine and Benzothiadiazole Moieties with Different Terminal Groups. *Dye. Pigment.* **2013**, *98*, 464–470.

(66) Chen, C.; Maldonado, D. H.; Le Borgne, D.; Alary, F.; Lonetti, B.; Heinrich, B.; Donnio, B.; Moineau-Chane Ching, K. I. Synthesis of Benzothiadiazole-Based Molecules: Via Direct Arylation: An Eco-Friendly Way of Obtaining Small Semi-Conducting Organic Molecules. *New J. Chem.* **2016**, *40*, 7326–7337.

(67) Zhang, Y.; Kim, B.; Yao, S.; Bondar, M. V. Controlled Aggregation and Enhanced Two-Photon Absorption of a Water-Soluble Squaraine Dye with a Poly(acrylic Acid) Template. *Langmuir* **2013**, *29*, 11005–11012.

(68) Sakae, H.; Nagatani, H.; Morita, K.; Imura, H. Spectroelectrochemical Characterization of Dendrimer − Porphyrin Associates at Polarized Liquid | Liquid Interfaces. *Langmuir* **2014**, *30*, 937–945.

(69) Oikawa, H.; Nakanishi, H. Reprecipitation Method for Organic Nanocrystals. In *Single Organic Nanoparticles*; Masuhara, H., Nakanishi, H., Sasaki, K., Eds.; Springer-Verlag: Berlin, 2003; pp 17–31.

(70) Ponterini, G.; Vanossi, D.; Krasnaya, Z. A.; Tatikolov, A. S.; Momicchioli, F. Electronic Spectra and (Hyper)polarizabilities of Non-Centrosymmetric D-A-D Chromophores. An Experimentally Based Three-State Model and a Theoretical TDDFT Study of Ketocyanines. *Phys. Chem. Chem. Phys.* **2011**, *13*, 9507–9517.

(71) Sissa, C.; Painelli, A.; Blanchard-Desce, M.; Terenziani, F. Fluorescence Anisotropy

Spectra Disclose the Role of Disorder in Optical Spectra of Branched Intramolecular-Charge-Transfer Molecules. *J. Phys. Chem. B* **2011**, *115*, 7009–7020.

(72) Greenspan, H.; Fischer, E. Viscosity of Glass-Forming Solvent Mixtures at Low Temperatures. *J. Phys. Chem.* **1965**, *69*, 2466–2469.

(73) Allouche, J. Synthesis of Organic and Bioorganic Nanoparticles: An Overview of the Preparation Methods. In *Nanomaterials: A Danger or a Promise? A Chemical and Biological Perspective*; Brayner, R., Flévet, F., Coradin, T., Eds.; Springer-Verlag: London, 2013; pp 27–74.

(74) Kuhn, H.; Kuhn, C. J-Aggregates; Kobayashi, T., Ed.; World Scientific: Singapore, 1996.

(75) Momicchioli, F.; Ponterini, G.; Vanossi, D. Linear and Nonlinear Optical Properties of V-Shaped D-π-A-π-D Chromophores: Effects of the Incorporation of Aromatic Rings in the Polyenic π-Bridges of Open-Chain Ketocyanines. *Phys. Chem. Chem. Phys.* **2014**, *16*, 15576–15589.

(76) Knoester, J. Optical Properties of Molecular Aggregates. In *Organic Nanostructures: Science and Applications*; IOS Press: Amsterdam, 2002.

(77) Nielsen, C. B.; White, A. J. P.; McCulloch, I. Effect of Fluorination of 2,1,3-Benzothiadiazole. *J. Org. Chem.* **2015**, *80*, 5045–5048.

(78) Langis-Barsetti, S.; Maris, T.; Wuest, J. D. Molecular Organization of 2,1,3-Benzothiadiazoles in the Solid State. *J. Org. Chem.* **2017**, *82*, 5034–5045.

(79) Kitamura, C.; Saito, K.; Ouchi, M.; Yoneda, A.; Yamashita, Y. Synthesis and Crystal Structure of 4,7-Bis (2-Thienylethynyl)-2,1,3-Benzothiadiazole. *J. Chem. Res.* **2002**, *10*,

511–513.

TOC Graphic